Focused Ion Beam Fabrication and Atomic Force Microscopy Characterization of Micro/Nanoroughness Artifacts With Specified Statistic Quantities

Yuhang Chen, Tingting Luo, and Wenhao Huang

***Abstract*—Series of roughness patterns with predetermined statistic quantities, such as standard deviation of surface heights, autocorrelation length, and height distribution were fabricated by focused ion beam (FIB) lithography and characterized by atomic force microscopy (AFM). Template-matching analysis and comparisons of surface parameters were performed to ascertain the fabrication and measurement qualities. Results show that the root-mean-square (rms) residuals are approximately 4.8, 5.2, and 15.7 nm for the fabricated Gaussian, negatively skewed, and positively skewed surfaces with the dimension of 5120 nm $\times$ 5120 nm $\times$ 121 nm. For the surfaces with the same skewness but different autocorrelation lengths, the rms residuals have no significant differences. The surface parameters of the fabricated artifacts are in close agreements with their expected values. To further elucidate the geometric interactions between the tip and roughness structure in AFM measurements, blind tip estimations were carried out on the scanned images. The tip estimation deviation increases with the increase of autocorrelation length for the Gaussian surfaces. The skewed structures help to improve the estimation accuracy. By a proper design of the surface quantities, the artifacts can serve as reference areal roughness standards at the nanoscale and a kind of tip characterizers.**

***Index Terms*—Atomic force microscopy (AFM), nanofabrication, nanostructures, scanning probe microscopy, surface roughness.**

I. Introduction

SURFACE structures are closely relevant to various functional performances of certain devices, such as adhesion, lubrication, antireflection, and electric contact. Consequently, quantitative measurements of the surface areal roughness are of critical importance in many fields of micro/nanotechnologies [1]. To characterize surface topography, scanning probe microscopy (SPM), including scanning tunneling microscopy (STM) and atomic force microscopy (AFM), has been realized as a category of promising tools [2]. Especially, AFM has drawn considerable interests because of the feasibility in measuring numerous kinds of specimens and the ultrahigh spatial resolution.

However, in view of quantitative surface nanometrology, AFM suffers several systematic disadvantages [3]. First, the surface measurements involve complex geometric interactions between the sample structure and the probe tip. Such couplings are relevant to the tip size, surface autocorrelation length, and surface heights and their distribution [4]. Even with the tip shape and instrument behaviors in three coordinate axes calibrated, quantitative roughness parameters are still difficult to be analyzed. Without prior knowledge of the sample structure, the manner of tip dilations cannot be precisely interpreted. Due to this limitation, even surface reconstructions with a known tip can occasionally fail to lead to better roughness evaluations [5]. Second, the local tip-sample forces, which are used for sensing the separation, might be different from point to point in the raster scan. Therefore, the distance between the tip apex and surface may be altered whereas it is assumed to be kept constant under feedback control. The measured topography will be distorted by these variations of physical properties. In dynamic mode AFM, the presence of nonlinear attractive and repulsive forces may cause bistability in the probe oscillations and induce image artifacts under some experimental conditions [6], [7]. To achieve reproducible measurements with high precision, the force effect should be carefully taken into consideration [8]. Third, the acquisition settings affect the obtained results dramatically. Reliable surface imaging requires a proper selection of feedback parameters [9], [10]. Last, the environmental factors including drift can affect quantitative roughness evaluations [11], especially when the surface spatial or slope/curvature properties are of interest. In addition, a lot of conventional roughness parameters are scale relevant. They are sensitive to the scan range and measurement resolution [12], [13]. The quantitative roughness characterization via AFM, particularly when the sample surface is ultrasmooth, is an important but rather complex matter.

To validate the surface roughness evaluations and ensure a more in-depth understanding of various influencing factors, reference artifacts with defined topography and prescribed statistic quantities are urgently demanded. However, the developments of irregular roughness standards and corresponding

Manuscript received August 5, 2013; revised December 21, 2013 and January 27, 2014; accepted February 27, 2014. Date of publication March 11, 2014; date of current version May 6, 2014. This work was supported by the "973" Project (No. 2011CB932801), the National Natural Science Foundation of China (No. 51275503 and No. 91023021). The review of this paper was arranged by Associate Editor L. Dong.

The authors are with the Department of Precision Machinery and Precision Instrumentation, University of Science and Technology of China, Hefei 230026, China (e-mail: chenyh@ustc.edu.cn; ltt@mail.ustc.edu.cn; whuang@ustc.edu.cn).

Color versions of one or more of the figures in this paper are available online at http://ieeexplore.ieee.org.

Digital Object Identifier 10.1109/TNANO.2014.2311103

characterization methods are fewer compared with regular calibration artifacts such as periodic one-dimensional and two-dimensional gratings. So far, only a few roughness patterns with micro/nanodimensions have been fabricated by nanomachine [14], electron beam lithography (EBL) [15], and direct laser writing (DLW) [16]. The artifacts developed via these techniques suffer some considerable problems. For the structures manufactured by nanomachine, the dimension is in the order of several hundred micrometers whereas such a size generally exceeds the measurable range of common probe microscopes. Moreover, current fabrication resolution may be insufficient for the SPM capability. For the EBL and DLW techniques, the roughness structures are written on polymers. Precise transfers of the complex three-dimensional (3-D) irregular structures to more stable materials are necessary, which are a great challenge on account of the strict requirements in spatial resolution and 3-D fidelity.

To further reduce the characteristic dimensions of the reference roughness artifacts and improve the structure stabilities, here we use focused ion beam (FIB) to fabricate a series of patterns with defined statistic quantities. As a prototype, the autocorrelation function and the surface height distribution are mainly controlled. The artifacts are produced directly on a silicon substrate. Compared with the patterns on polymers coated with metals, namely those manufactured by EBL and DLW, the structure stability can be improved. Also, the fabrication resolution can easily reach several nanometers, which is suitable for applications in SPM. To quantify the fabrication quality, AFM characterizations are adopted. Template matching analysis and evaluations of surface parameters are carried out. The geometric interactions of the finite tip shape and the roughness structure are considered. As a reverse problem, blind tip estimations on the measured images are addressed, and compared with the scanning electron microscopy (SEM) measurements. The developments of the roughness artifacts and analysis methods are toward the purpose of ascertaining SPM areal roughness evaluations. Such a kind of artifacts can reflect practical roughness measurement situations more accurately. On the other hand, they have well-defined multi-frequency surface components. Rich information on the instrumental responses at different spatial frequencies can be also provided in characterizations. Furthermore, the structures with controllable surface parameters are capable of supporting more quantitative experimental investigations of numerous roughness relevant functional performances.

II. Experiments

A. Rough Surface Generation

It has been well recognized that some of the most important geometric properties of a surface can be characterized by its height distribution and autocorrelation function [17]. Surface topographic data can be reasonably generated by statistical modeling. Here, we use conventional digital filter and fast Fourier transformation method for the rough surface simulation [18]. In the design, the autocorrelation function is assumed to be in the form of,

$$Rz(x,y) = \sigma^2 \exp\left\{-2.3\left[\left(\frac{x}{\lambda_x}\right)^2 + \left(\frac{y}{\lambda_y}\right)^2\right]\right\}. \quad (1)$$

In this equation, σ is the standard deviation of the surface heights, and λ_x and λ_y are the autocorrelation lengths in the x and y directions, respectively. The surface is spatially isotropic, that is, $\lambda_x = \lambda_y$. The autocorrelation function is specified as an exponential decay with the coefficient set to reach 0.1 decrease at the autocorrelation length. Then, a two-dimensional digital filter is designed according to (1) and a random sequence with assigned moments is filtered to obtain the rough surface. For the non-Gaussian surface generation, parameters skewness (S_{sk}) and kurtosis (S_{ku}) are employed to control the height distribution. These two parameters should always satisfy [16]

$$S_{ku} - S_{sk}^2 - 1 \geq 0. \quad (2)$$

Depending on the nonzero skewness, the surface structure will be either peak or valley dominant.

To improve the design accuracy, i.e., to reduce the discrepancies between the characterization parameters of the numerically generated surface and their corresponding expected values, combinations of genetic algorithms are applied for optimization [15]. Consequently, the rough surfaces have well-defined statistic quantities, such as autocorrelation length, skewness, and kurtosis. After the optimal design, fiduciary markers or guidance patterns can be associated with the effective structures for easy location and orientation.

Three types of patterns are generated, which are the rough surfaces with negatively skewed, Gaussian, and positively skewed height distributions. The skewnesses are selected as $-1, 0$, and 1, respectively. The kurtosis of every non-Gaussian surface equals to 5. The skewness and kurtosis satisfy the general restriction described in (2). In each series of patterns with the same height distribution, the fastest decay autocorrelation lengths are different. They are 200, 320, 400, and 500 nm, respectively. All the surfaces have a developed area of 5.12 μm $\times$ 5.12 μm, which corresponds to 512 pixels $\times$ 512 pixels in the numerical simulation. The peak-to-valley surface heights are determined to be approximately 121 nm. However, there would be a certain deviation for a particular random rough surface.

B. FIB Fabrication

In FIB fabrication, the designed surface data are converted into a bitmap first. Then, the fluence of the ion beam at each pixel is evaluated according to the grayscale level, that is, the surface height at the corresponding position. Upon the focused gallium ion irradiation, the materials on the silicon substrate will be ablated. In our experiments, mainly the dwell time at each pixel is altered to induce the desired etching depth. After the raster scan while varying the ion fluence simultaneously, the entire roughness pattern is etched pixel by pixel in a controllable way. The scan procedure is repeated twice to develop the final structure.

The fabrication is performed on a FIB/SEM dual beam system (FEI Nova 200 Nanolab). The resolution is approximately 7 nm

at the acceleration voltage of 30 kV. The beam current is fixed at 300 pA for all the experiments. The dose G_{dose} in ions/cm^2 can be calculated according to (3) for an ion current I_{ion} of the gallium source in pA, exposure time t_{exposure} in s, and pattern area A_{pattern} in μm^2 [19]

$$G_{\mathrm{dose}} = \frac{I_{ion} \times t_{\mathrm{exposure}}}{A_{\mathrm{pattern}} \times 1.602 \times 10^{-15}}. \tag{3}$$

The experimental incident dose is determined to be approximately 1.7×10^{17} ions/cm^2. The magnitude is within the optimal range for the nanoscale fabrication on the silicon material, which has been well investigated by taking various influencing factors into account [19]. The artifacts are SEM imaged *in situ* after the lithography, toward the purpose of providing clues to optimize the processing parameters. The over bombardment is avoided. The maximum dwell time for exposing one pixel is definitively optimized to be 95 μs for the Gaussian rough surfaces, 130 μs for the negatively skewed surfaces, and 70 μs for the positively skewed surfaces.

C. AFM Characterization

For quantitative evaluations, we employed the AFM (Bruker Innova) to measure the roughness specimens. Two types of probes have been adopted. The first one is the RTESPA-CP probe (Bruker Corporation), which has a nominal resonance frequency of 358 kHz and a spring constant of 20 N/m. The second one is the ARROW-FMR probe (NanoWorld Services) with a resonance frequency of 75 kHz and a spring constant of 2.8 N/m. Hereafter, we denote the two probes as the C1 and C2 probes. The probes are imaged by SEM to determine the geometry and size. The C1 probe tip is found to have a smaller cone angle than the C2 probe tip. The AFM data scanned by the C2 probe are then mainly used for blind tip estimation since more tip dilations are assumed to be involved.

The images were acquired in tapping mode to reduce tip wear and sample damage. In order to cover the whole region of the effective roughness pattern, the scan area was selected as 8.0 μm $\times$ 8.0 μm. The sampling points were 512 pixels $\times$ 512 pixels and the scan rate was set as 0.6 Hz. The time needed for scanning one image in this case is about 853.3 s, which is quite a long duration. The possible influence of drift should be carefully paid attention. By analyzing a pair of counter-scanned images [20], the drift was found to have no significant distortions in our AFM characterizations. Its influence was safely ignored in the following analysis. The raw acquired topography data were imported into the WSXM software for image presentation and processing [21].

III. Results and Discussion

To ascertain the FIB fabrication quality and highlight the tip-sample geometric coupling in the AFM characterization, several validation methods have been applied. First, visual image comparisons of the measured and designed surfaces are conducted. Second, precise template matching evaluations are carried out. Third, roughness parameters from various geometric aspects are compared. Last, blind tip estimation accuracies on the scanned AFM images are discussed, which inversely indicates the amount of possible tip distortions.

A. Image Comparison

The FIB fabricated artifacts with controlled statistic characteristics are shown in Figs. 1–3. The C1 probe was used in the AFM measurements. In Fig. 1, we depict the surfaces with a Gaussian height distribution. Their autocorrelation lengths are 200, 320, 400, and 500 nm, respectively. The scanned data were cropped to extract only the effective roughness area and then aligned to the design template manually for clarity. Intuitively, we can make two determinations. First, the acquired topography matches well with the design template. One-to-one correspondence of the concave and convex structures can be unambiguously observed. Second, tip dilations on the surface with the autocorrelation length of 200 nm are much more severe than those on the surfaces with larger autocorrelation lengths. Note that these four samples have similar amplitude properties.

Fig. 2 illustrates the roughness artifacts with the negative skewness of -1. A negative skewness indicates the preponderance of surface valleys against peaks. Accordingly, the images are dominated by bright areas, which mean higher surface heights in shading. Again, the measured data coincide very well with the design template and the tip dilations on the surface with a smaller autocorrelation length are much more obvious. These preliminary comparisons verify that the FIB technique has remarkable fidelity and resolution in generating the complex 3-D patterns.

The fabrication results of the rough surfaces with the positive skewness of 1 are shown in Fig. 3. Compared with the surfaces with a zero or negative skewness, larger deviations between the designed and fabricated patterns are observed. Two main factors can contribute to the phenomena. First, sharp peaks are the dominant structures in a positively skewed surface while the FIB fabrication of sharp peaks might be sensitive to the nonvanishing finite size of the focused beam, the positioning error, and the repeatability. Remember that the raster scan was repeated twice in the experiments. The other is more severe tip dilations on the sharp peaks in AFM scanning [4]. However, apparent discrepancies appear even in case of surfaces with a larger autocorrelation length where tip distortions are assumed to be smaller. The fabrication error is then considered to be the most likely contribution. Further improvements should be taken to enhance the stability and the positioning accuracy in FIB processing. Though the deviation is obvious, the similarity remains for each pair of surfaces.

B. Surface Template Matching

With the AFM data, quantitative evaluations can be carried out. For a comprehensive examination of the FIB fabrication quality, the measured data and the design template should be compared. It is worthy to mention that their coordinate systems are not necessarily the same due to different sample tilts, scan directions, scan areas, and sampling intervals in AFM measurements. The comparison cannot be realized by a simple subtraction operation, and so we performed the template matching first.

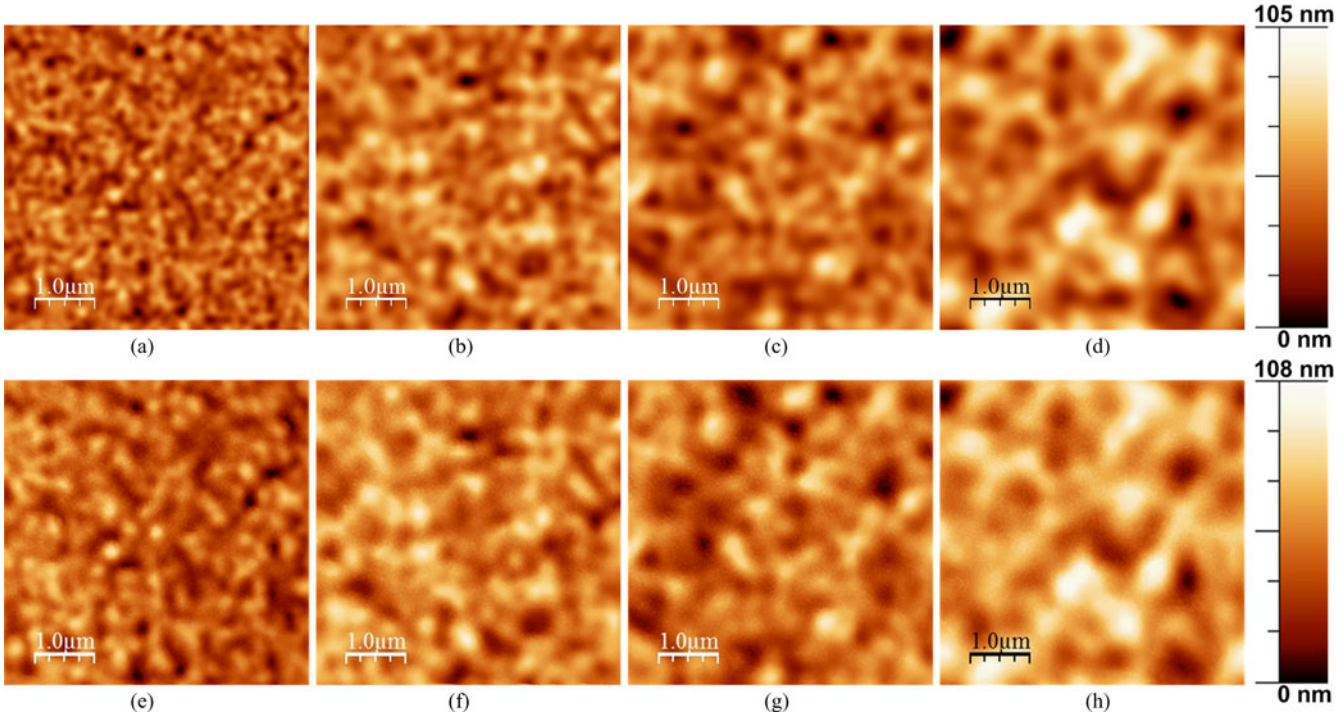

Fig. 1. FIB fabrication results of the roughness artifacts with Gaussian surface height distribution. (a)–(d) Design templates. The autocorrelation lengths are 200, 320, 400, and 500 nm, respectively. (e)–(h) Corresponding measured AFM images.

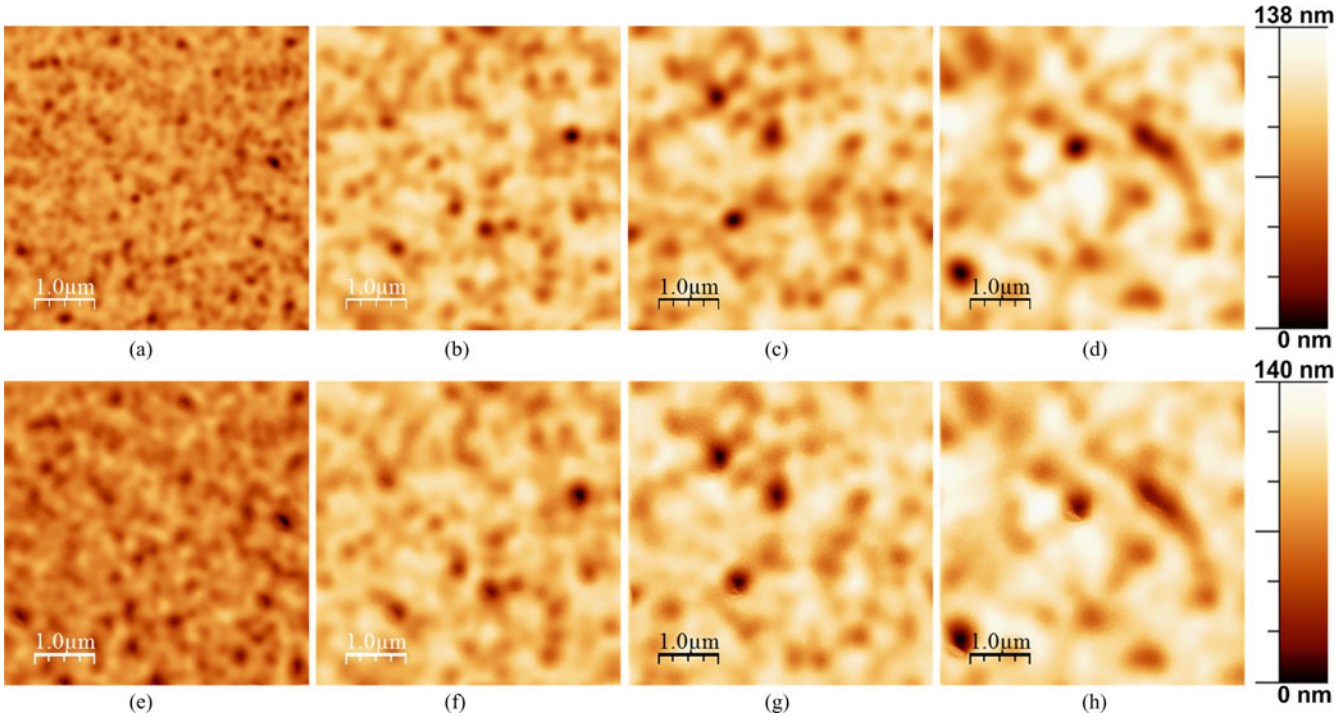

Fig. 2. FIB fabrication results of the roughness artifacts with the negative skewness of –1. (a)–(d) Design templates. The autocorrelation lengths are 200, 320, 400, and 500 nm, respectively. (e)–(h) Corresponding measured AFM images.

Considering the practical experimental conditions, only the rigid translation and rotation between the two data sets are taken into account whereas the possible shear and affine transformations are neglected for the sake of simplicity.

The design template contains discrete coordinate data. In the matching, the template is fitted into a nonuniform rational B-spline (NURBS) surface. The sum of the orthogonal distances from the measured data set, which is after optimal rotation and

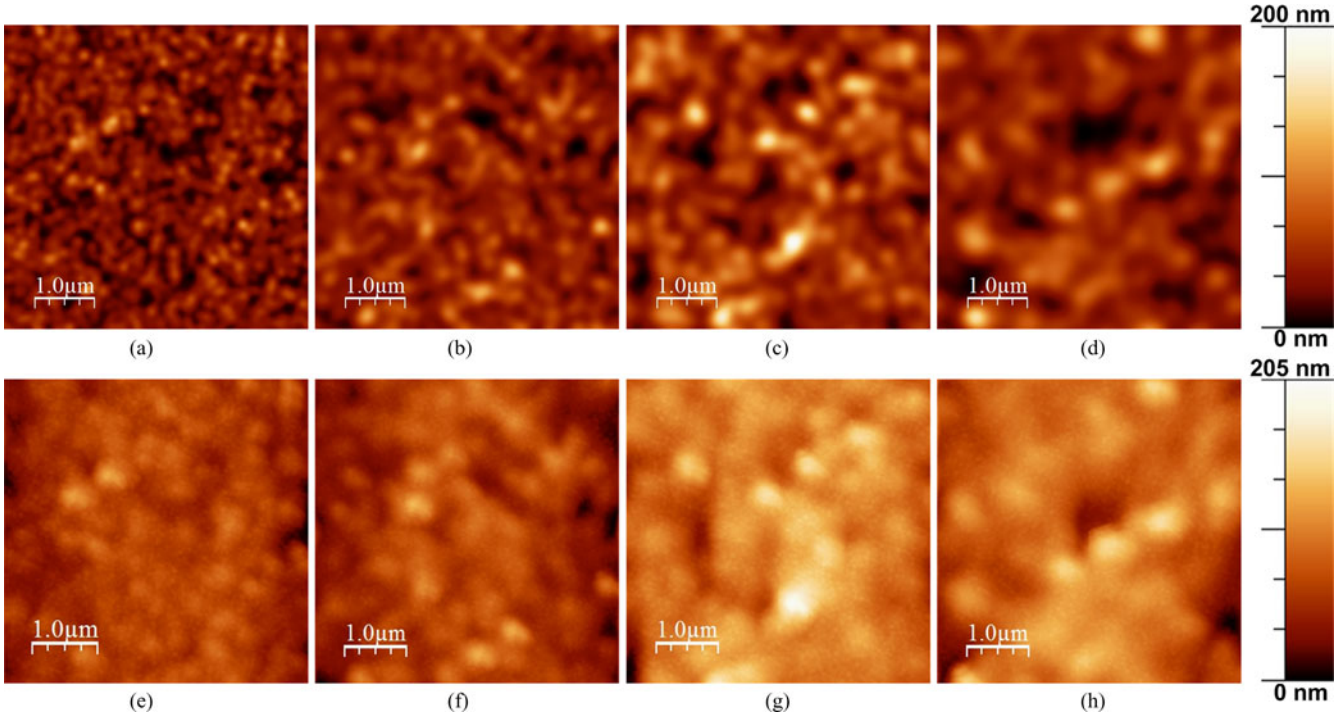

Fig. 3. FIB fabrication results of the roughness artifacts with the positive skewness of 1. (a)–(d) Design templates. The autocorrelation lengths are 200, 320, 400, and 500 nm, respectively. (e)–(h) Corresponding measured AFM images.

translation, to the NURBS surface is applied as an error metric [22]

$$E = \sum_{i=1}^{N} \|\mathbf{R}\mathbf{m}_i + \mathbf{T} - \mathbf{d}_i\|^2 \tag{4}$$

where $\mathbf{R}$ is the rotation matrix and $\mathbf{T}$ is the translation vector. $\mathbf{M} = \{\mathbf{m}_1, \mathbf{m}_2, \ldots, \mathbf{m}_N\}$ denote the measured data and $\mathbf{D} = \{\mathbf{d}_1, \mathbf{d}_2, \ldots, \mathbf{d}_N\}$ represent the projection points associated with $\mathbf{M}$ on the NURBS surface. The matching is solved iteratively to minimize the squared distance between the two surfaces by using the Levenberg–Marquardt algorithm. This derivative-based method, which employs continuous template functions, has been demonstrated to prevail against conventional iterative closest point method on the 3-D rough surface registration. Substantial improvements in both accuracy and efficiency can be achieved [23].

Typical residuals of the series of surfaces after template matching are shown in Fig. 4. From the results, the distributions of the residuals are quite isotropic. The spatial positions, where the residuals are larger, are in general accordance with the positions of the peaks and valleys. Compared with the skewed surfaces, the maxima of the local residuals calculated on the Gaussian surfaces are smaller. In addition, the influence of skewness on the fabrication accuracy seems to be larger than that of the autocorrelation length. The root-mean-square (rms) residuals of all the fabricated Gaussian and negatively skewed surfaces are in the same magnitude of approximately 5.0 nm, as presented in Table I. And the rms residual keeps almost constant when the autocorrelation length is varied. For the positively skewed surfaces, the rms residuals are approximately 15.7 nm, which are nearly three times of those obtained on the surfaces with a near zero or negative skewness. The quantitative evaluations verify the qualitative observations depicted in Figs. 1–3. The FIB fabrication of the complex 3-D patterns is demonstrated to have the nanoscale precision.

C. Surface Parameters Comparison

Though the template matching can provide a systematic evaluation among the sampled volume, the degree of agreement in the separated amplitude, spatial, and hybrid features remains not so clear from the analyzed residuals. Therefore, comparisons of a group of surface parameters are performed. According to the template matching result, the effective roughness region is firstly extracted and transformed. Then, the mean plane of the surface data is determined and subtracted. The surface roughness parameters are evaluated from the pre-processed data. We have calculated 14 popular parameters for each data set [15]. Fig. 5 demonstrates the results on some typical parameters. They are ten-point surface height S_z, skewness S_{sk}, autocorrelation length at the 0.2 decay S_{al20}, and rms surface slope S_{dq}. The ten-point height is the average difference between five highest peaks and five deepest valleys. These four parameters characterize surface amplitude, distribution, spatial and hybrid properties, respectively. They are adopted here to ascertain the fabrication quality from all these geometric aspects.

The deviation of the parameter ten-point height is generally satisfactory for each fabricated roughness pattern. The relative errors are in the range of -3.1% to 5.0%, -5.2% to 0.9%, and -12.2% to 10.9% for the Gaussian, negatively skewed, and positively skewed surfaces, respectively. The extreme amplitudes

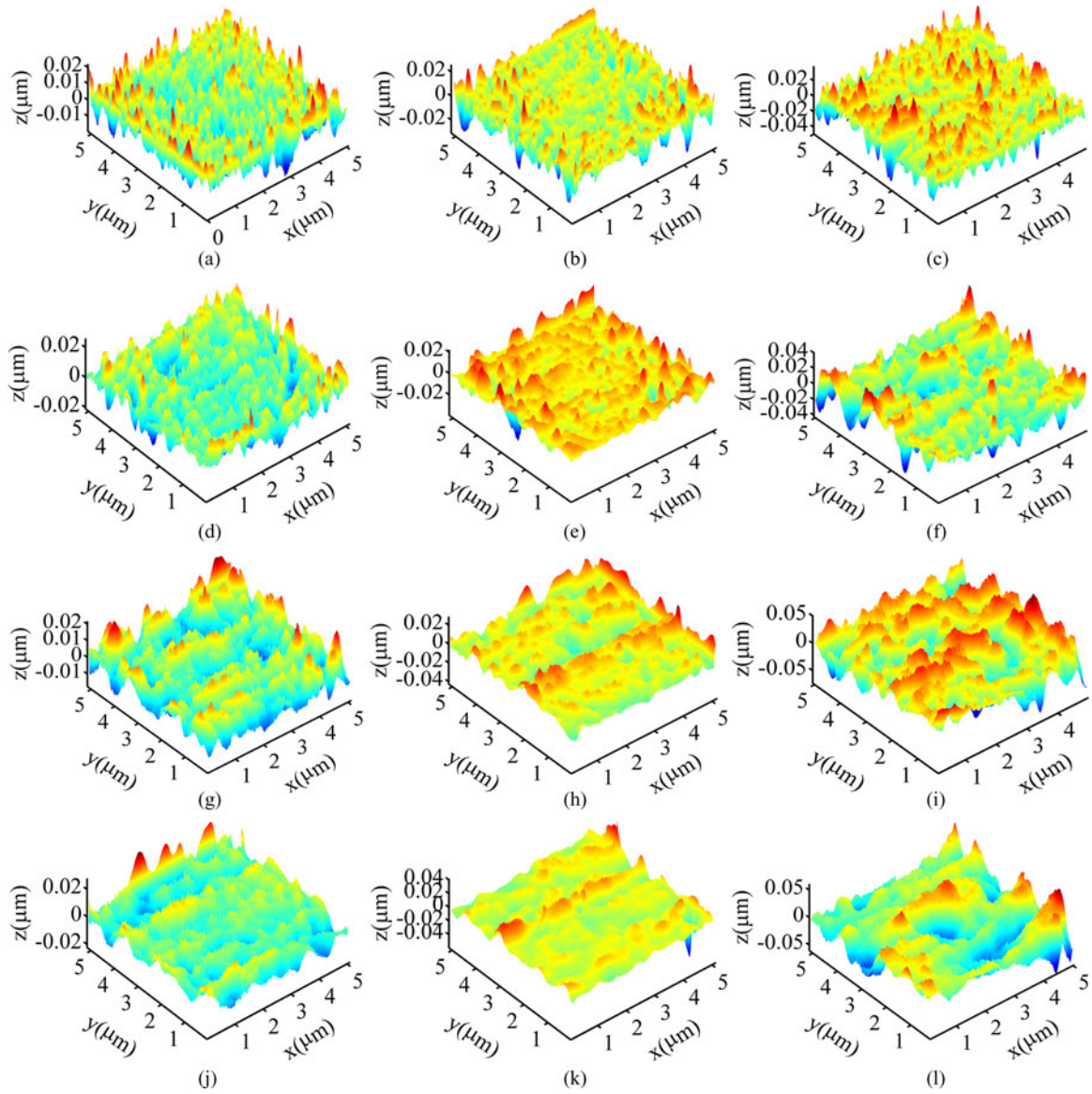

Fig. 4. Residuals of the measured surface after template matching. (a) Skewness $S_{sk} = 0$, autocorrelation length $\lambda = 200$ nm. (b) $S_{sk} = -1$, $\lambda = 200$ nm. (c) $S_{sk} = 1$, $\lambda = 200$ nm. (d) $S_{sk} = 0$, $\lambda = 320$ nm. (e) $S_{sk} = -1$, $\lambda = 320$ nm. (f) $S_{sk} = 1$, $\lambda = 320$ nm. (g) $S_{sk} = 0$, $\lambda = 400$ nm. (h) $S_{sk} = -1$, $\lambda = 400$ nm. (i) $S_{sk} = 1$, $\lambda = 400$ nm. (j) $S_{sk} = 0$, $\lambda = 500$ nm. (k) $S_{sk} = -1$, $\lambda = 500$ nm. (l) $S_{sk} = 1$, $\lambda = 500$ nm.

are accurately controlled. As to the parameter skewness, the deviation is smaller for the surface with a Gaussian distribution or a negative skewness, whereas a larger deviation is found for the surface with a positive skewness. The height distribution of the positively skewed surface is dramatically distorted. The comparison results on the fastest decay autocorrelation length are satisfactory for the both kinds of surfaces with zero and negative skewnesses whereas a large error is found for the surface with a positive skewness. A reason for the large divergence for the positive skewness of 1 may be, as discussed earlier, that sharp peaks are the dominant structures in such a surface and that these may have led to significant fabrication errors when using the FIB source. Concerning the parameter rms surface slope, the deviations are acceptable for all the fabricated surfaces. From the evaluations of another parameter rms roughness (S_q), the relative errors are found to be within the range of -6.3% to 9.1% for the surfaces with the skewness of 0 or -1. The errors are larger for the surfaces with the skewness of 1 and they almost increase to the range of -15.4% to 16.3%. Moreover, parameter S_q is less sensitive to noise and being the most stable in AFM characterization because it is the average amplitude.

TABLE I
RMS RESIDUALS OF THE MEASURED SURFACES

Root-mean-square residual (nm)				
Skewness	Autocorrelation length			
	200	320	400	500
0	5.0	4.9	5.0	4.2
-1	5.5	4.4	5.4	5.5
1	14.2	14.0	17.8	16.8

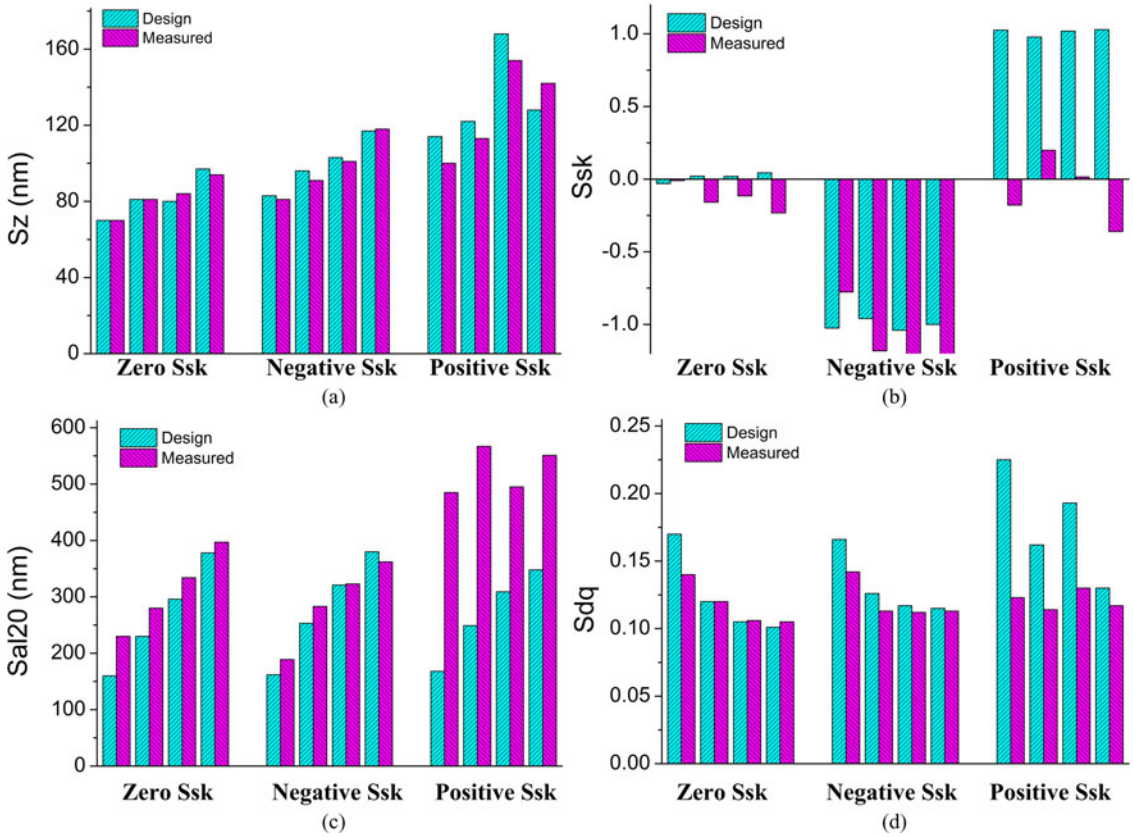

Fig. 5. Comparisons of typical parameters of the surfaces with different height distributions, namely, normal distribution (zero S_{sk}), negatively skewed (negative S_{sk}), and positively skewed (positive S_{sk}). Four surfaces with increasing autocorrelation length (from left to right) are evaluated in each series. (a) Ten-point height S_z, (b) skewness S_{sk}, (c) autocorrelation length at the 0.2 decay S_{al20}, and (d) rms surface slope S_{dq}.

Above results demonstrate that the surface amplitude, distribution, spatial, and hybrid properties are well recurred. The statistic quantities of the roughness patterns can be controlled with nanoscale accuracy. In general, the fabrication of the complex roughness artifacts through FIB method is quite promising. However, further optimizations of the fabrication procedures are demanded when a highly positively skewed surface is to be fabricated.

D. Blind Tip Estimation on Roughness Artifacts

The artifacts with controlled surface parameters can be adopted for the validation of nanoscale roughness evaluations and the elucidation of various influencing factors as reference materials. In SPM characterization, it is well known that tip dilations will significantly affect the roughness measurements [4], [5]. As a reverse problem, here we focus on analyzing the accuracy of blind tip estimation performed on the scanned surface data. Such an analysis can provide an indication of the amount of possible tip dilations and highlight the tip-sample geometric coupling in the measurements.

The finite tip size is recognized as one of the most important factors in SPM dimensional metrology, such as the measurements of surface roughness, line width, and particle size. The tip shape is also significant in other applications of the microscope, for example nanoindentation and electric characterization [24]. A critical problem is thus to determine the tip geometry. Certainly, one can measure the tip by SEM or transmission electron microscopy (TEM). But electron microscopy imaging is not convenient for *in situ* tip determination. Another alternative way is to scan the tip on known structures, such as nanotubes, nanoparticles, self-assembled monolayers, and comb-shaped specimens. These specially developed structures often severe as tip characterizers [25], [26]. Unfortunately, such off-line methods preclude *in situ* analysis on practical experimental samples. On the contrary, blind tip estimation is able to reconstruct the tip geometry only from the scanned image. It can be applied to all kinds of surfaces, either with or without defined structures. Mathematically, the tip estimation is solved in a nesting approach [27]

$$p_{k+1}(\mathbf{x}) = \min_{\mathbf{x}' \in D_I} \{ \max_{\mathbf{v} \in D_{p'}} \{ \min[i(\mathbf{x} + \mathbf{x}' - \mathbf{v}) + p_k(\mathbf{v}) - i(\mathbf{x}'), p_k(\mathbf{x})] \} \} \tag{5}$$

where i denotes the image and p denotes the reflected tip, $\mathbf{v}$ is the displacement vector of the tip at the point of $\mathbf{x}$ in the scanned AFM image, and k is the iteration step. Symbols D_I and $D_{p'}$ represent domains of the image and the reflected tip, respectively. The tip estimation procedure can be implemented flexibly since it does not require any prior knowledge of the sample topography [28].

The blind tip estimations using (5) are carried out with the Gwyddion software [29]. Fig. 6 presents the typical AFM

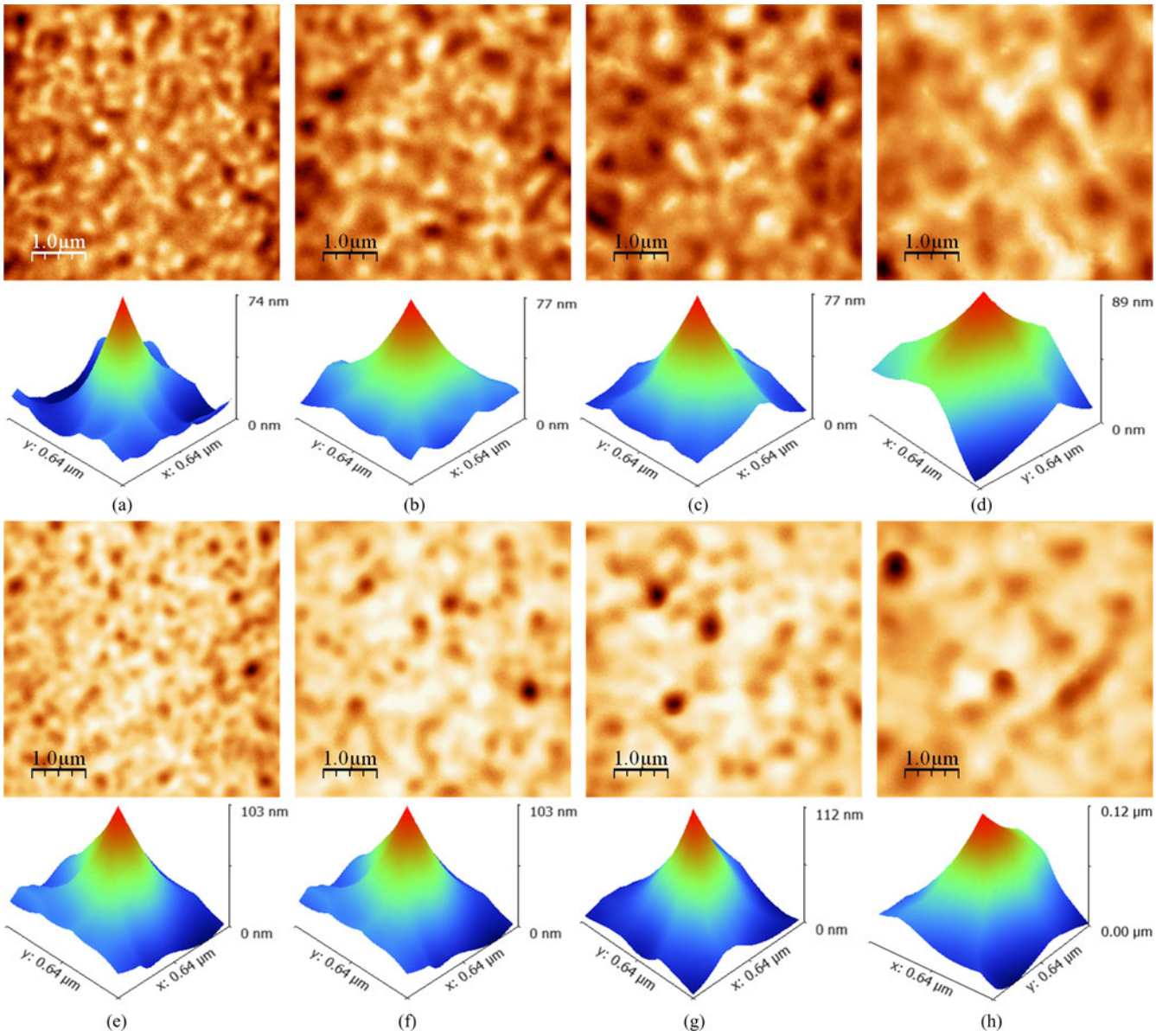

Fig. 6. Blind tip estimation on the AFM images of the surfaces with different parameters. (a)–(d) AFM images and estimated probes of the Gaussian surfaces with the autocorrelation lengths of 200, 320, 400, and 500 nm. (e)–(h) AFM images and estimated probes of the negatively skewed surfaces with the autocorrelation lengths of 200, 320, 400, and 500 nm.

images and the estimated tips. The adopted probe is the C2 type. In fact, the images are very similar to those acquired by the C1 probe. The three-sided pyramid geometry of the probe tip is reasonably reconstructed from each measured image but the tip size is different. In principle, blind tip estimation only provides an upper bound of the real tip geometry. Because the estimated tip is not necessarily close to its real size, a rough determination of the reliability of the achieved tip dimension is demanded.

In order to facilitate the discussion, we begin with analyzing the simplest case where a roughness profile is scanned. The rms curvature can be calculated from the spectral density, which is the Fourier transform of the autocorrelation function [30]. If the profile has a Gaussian spectrum, the rms curvature can be approximated as shown

$$\gamma = \alpha \frac{\sigma}{\lambda^2} \tag{6}$$

where α is a constant. For an autocorrelation function in the form of (1), the factor α is determined to be $3^{1/2}(2/\pi)^{1/4} \times 2.3$. The rms curvature is quite sensitive to the variation of the autocorrelation length λ. When only the geometric interactions are taken into account, two major factors are reasonably assumed to affect the accuracy of blind tip estimation. The first is the ratio of tip curvature to surface rms curvature. If the ratio is extremely small, the tip can fail to trace the profile faithfully because the coupled tip information is significant [31]. Therefore, the blind tip estimation performed on the acquired image will be

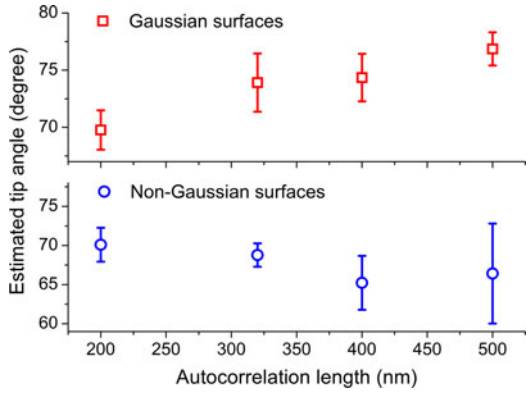

Fig. 7. Estimated half-cone angle of the tip when the surface autocorrelation length increases.

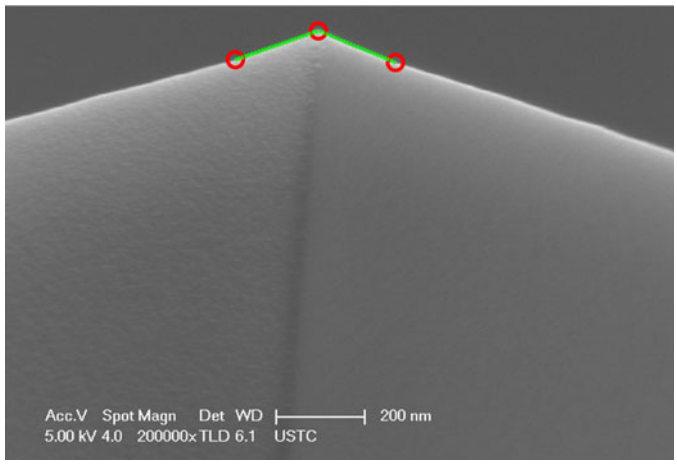

Fig. 8. SEM image of the probe adopted for AFM imaging. The cone angle is measured automatically.

relatively accurate. That is to say, the accuracy is associated with the amplitude and spatial surface parameters of the sample. The other factor is the height distribution. The dominance of peaks or valleys in a highly skewed surface will cause larger tip dilations and help to improve the tip estimation accuracy. In total, the validity of the numerically analyzed probe tip can be determined by

$$\xi \propto \chi \frac{\lambda^2}{\sigma R_{\text{real}}} \tag{7}$$

where ξ denotes the tip estimation error and χ is a factor relevant to the height distribution. R_{real} denotes the actual tip radius.

Due to the large scan size of 8 μm $\times$ 8 μm and the limited sampling points of 512 pixels $\times$ 512 pixels in the acquired image, the very tip apex fails to be estimated. Moreover, the nominal tip radius is smaller than 10 nm. As a result, the half-cone angle is more suitable to quantify the tip size than the apex radius in this case. The cone angles along all the directions in the pyramid structures are then calculated. The mean half-cone angles and their standard deviations are shown in Fig. 7. The estimated tip angle is determined to be 69.8° $\pm$ 1.7° for the Gaussian surface with the autocorrelation length of 200 nm. The half-cone angle gradually increases up to 76.9° $\pm$ 1.5° when the autocorrelation length increases to 500 nm. The increment is obvious and the general tendency is in accord with the simple analysis presented in (7). The above results suggest the sample surfaces with larger autocorrelation lengths are beneficial for the precise measurements if other conditions are the same. Characterizations of thin film roughness have already demonstrated that the amplitude and spatial surface parameters measured by AFM are acceptable as long as the radius of the major features in the image is several times of the tip radius [32]. Such an indication is in accord with the conclusion made from above tip estimations. For the non-Gaussian surface with the autocorrelation length of 200 nm, the estimated tip angle is 70.1° $\pm$ 2.2°. The mean value of the estimated tip angle is free of significant variation while its standard deviation becomes larger when the autocorrelation length increases. If a rough surface with a highly skewed height distribution is scanned, the tip dilations are dramatic at the dominated sharp peaks or deep valleys. Consequently, the blind tip estimation is much more accurate. However, depending on whether sufficient peaks or valleys present in a certain direction or not, the estimated tip profile could be randomly deviated.

For verification of the blind tip estimation, we compared the results with SEM experiments. From the photograph presented in Fig. 8, we can find that the C2 probe tip is exactly in the three-sided pyramid form. The two very edges of the tip were then tracked automatically by using a custom-written program. A least square linear fit of each extracted edge was applied and the angle between the two fitted lines was calculated. The half-cone angle was finally determined to be 69.1°. The magnitudes obtained by blind tip estimations performed on the surfaces with the autocorrelation length of 200 nm are in well accordance with the value obtained by SEM image analysis. Both the tip geometry and size have been precisely determined. It should be mentioned that the estimated tip angle of the sharp C1 probe tip is much greater than the SEM measured one. Compared with the actual angle of approximately 25.0°, the relative deviations are in the range of 40.2% to 54.8%. The increment of the estimation error can be expected when the real tip is sharper, as demonstrated in (7). On the other hand, the dependence of estimation accuracy on the surface autocorrelation length is the same as the C2 probe tip. It is hoped that the roughness artifacts may be additionally adopted as a kind of tip characterizers by controlling the height distributions and autocorrelation functions of the design surfaces properly. From the geometric point of view, decreasing the surface autocorrelation length and increasing the absolute skewness will enhance the precise tip estimation.

IV. Conclusion

In conclusion, a series of roughness patterns at the micro/nanoscale with specified statistic quantities were fabricated by FIB lithography. Template matching was performed to ascertain the FIB fabrications and AFM measurements. Results show the typical residuals of the Gaussian, negatively skewed, and positively skewed surfaces are approximately 4.8, 5.2, and 15.7 nm at the full dimension of 5120 nm $\times$ 5120 nm $\times$ 121 nm. For the surfaces with the same skewness but different

autocorrelation lengths, the rms residuals have no significant differences. Fabrications of Gaussian and negatively skewed surfaces seem to be more accurate than positively skewed surfaces. Evaluations of several surface parameters, which characterize the surface amplitude, horizontal, and hybrid geometric properties, demonstrate that the roughness characteristics can be precisely controlled except for the surfaces with a large positive skewness. In general, the FIB fabrications of the complex 3-D roughness structures are satisfactory.

To further reveal the geometric coupling of the tip and sample in AFM measurement, blind tip estimations on the scanned images were also carried out. The estimated tip shape and size are in accord with the SEM determinations. The tip estimation error increases with the increase of autocorrelation length and the skewed surfaces help to improve the accuracy. By a proper design of height distribution and autocorrelation length, the roughness artifacts may be additionally adopted as a kind of tip characterizers.

After necessary improvements, the developed artifacts can serve as reference roughness specimens for validating the surface areal roughness evaluations at the nanometer scale and supporting more quantitative experimental investigations on the functional performances, which are correlated to the surface roughness. The irregular artifacts have a potential for applications in surface nanometrology and a variety of relevant research areas.

REFERENCES

[1] R. Venkatasubramanian, K. Jin, and N. S. Pesika, "Use of electrochemical deposition to create randomly rough surfaces and roughness gradients," *Langmuir*, vol. 27, no. 7, pp. 3261–3265, Apr. 2011.

[2] A. Yacoot and L. Koenders, "Recent developments in dimensional nanometrology using AFMs," *Meas. Sci. Technol.*, vol. 22, no. 12, p. 122001, Dec. 2011.

[3] A. Yacoot and L. Koenders, "Aspects of scanning force microscope probes and their effects on dimensional measurement," *J. Phys. D: Appl. Phys.*, vol. 41, no. 10, p. 103001, May 2008.

[4] Y. Chen and W. Huang, "Numerical simulation of the geometrical factors affecting surface roughness measurements by AFM," *Meas. Sci. Technol.*, vol. 15, no. 10, pp. 2005–2010, Oct. 2004.

[5] C. Wang and H. Itoh, "A simulation study for evaluating and improving the accuracy of surface roughness measured by atomic force microscopy," *Meas. Sci. Technol.*, vol. 24, no. 3, p. 035401, Mar. 2013.

[6] S. Santos, V. Barcons, J. Font, and N. H. Thomson, "Bi-stability of amplitude modulation AFM in air: Deterministic and stochastic outcomes for imaging biomolecular systems," *Nanotechnology*, vol. 21, no. 22, p. 225710, Jun. 2010.

[7] Y. Chen and W. Huang, "Automatic glitch elimination of scanning probe microscopy images," *Anal. Sci.*, vol. 27, no. 2, pp. 153–156, Feb. 2011.

[8] T. Kowalewski and J. Legleiter, "Imaging stability and average tip-sample force in tapping mode atomic force microscopy," *J. Appl. Phys.*, vol. 99, no. 6, p. 064903, Mar. 2006.

[9] J. F. G. Martinez, I. Nieto-Carvajal, J. Abad, and J. Colchero, "Nanoscale measurement of the power spectral density of surface roughness: How to solve a difficult experimental challenge," *Nanaoscale Res. Lett.*, vol. 7, no. 1, p. 174, Mar. 2012.

[10] M. W. Fairbairn and S. O. R. Moheimani, "A switched gain resonant controller to minimize image artifacts in intermittent contact mode atomic force microscopy," *IEEE Trans. Nanotechnol.*, vol. 11, no. 6, pp. 1126–1133, Nov. 2012.

[11] N. D. Follin, K. D. Taylor, C. J. Musalo, and M. L. Trawick, "Three-axis correction of distortion due to positional drift in scanning probe microscopy," *Rev. Sci. Instrum.*, vol. 83, no. 8, p. 083711, Aug. 2012.

[12] J. D. Kiely and D. A. Bonnell, "Quantification of topographic structure by scanning probe microscopy," *J. Vac. Sci. Technol. B*, vol. 15, no. 4, pp. 1483–1493, Jul. 1997.

[13] R. Hristu, S. G. Stanciu, G. A. Stanciu, I. Capan, B. Guner, and M. Erdogan, "Influence of atomic force microscopy acquisition parameters on thin film roughness analysis," *Microsc. Res. Tech.*, vol. 75, no. 7, pp. 921–927, Jul. 2012.

[14] K. Nemoto, K. Yanagi, M. Aketagawa, I. Yoshida, M. Uchidate, T. Miyaguchi, and H. Maruyama, "Development of a roughness measurement standard with irregular surface topography for improving 3D surface texture measurement," *Meas. Sci. Technol.*, vol. 20, no. 8, p. 084023, Aug. 2009.

[15] X. Liu, T. Luo, Y. Chen, W. Huang, and G. Piaszenski, "Optimal design and fabrication of three-dimensional calibration specimens for scanning probe microscopy," *Rev. Sci. Instrum.*, vol. 83, no. 5, p. 053708, May 2012.

[16] T. Luo, X. Liu, Y. Chen, W. Huang, and Z. Liu, "Design and laser fabrication of controllable non-Gaussian roughness surfaces at microscale," *Appl. Surf. Sci.*, vol. 276, pp. 95–100, Jul. 2013.

[17] K. K. Manesh, B. Ramamoorthy, and M. Singaperumal, "Numerical generation of anisotropic 3D non-Gaussian engineering surfaces with specified 3D surface roughness parameters," *Wear*, vol. 268, no. 11, pp. 1371–1379, May 2010.

[18] M. Uchidate, K. Yanagi, I. Yoshida, T. Shimizu, and A. Iwabuchi, "Generation of 3D random topography datasets with periodic boundaries for surface metrology algorithms and measurement standards," *Wear*, vol. 271, no. 3, pp. 565–570, Jun. 2011.

[19] B. D. Huey and R. M. Langford, "Low-dose focused ion beam nanofabrication and characterization by atomic force microscopy," *Nanotechnology*, vol. 14, no. 3, pp. 409–412, Mar. 2003.

[20] R. V. Lapshin, "Automatic drift elimination in probe microscope images based on techniques of counter-scanning and topography feature recognition," *Meas. Sci. Technol.*, vol. 18, no. 3, pp. 907–927, Mar. 2007.

[21] I. Horcas, R. Fernandez, J. M. Gomez-Rodriguez, J. Colchero, J. Gomez-Herrero, and A. M. Baro, "WSXM: A software for scanning probe microscopy and a tool for nanotechnology," *Rev. Sci. Instrum.*, vol. 78, no. 1, p. 013705, Jan. 2007.

[22] X. Jiang, X. Zhang, and P. J. Scott, "Template matching of freeform surfaces based on orthogonal distance fitting for precision metrology," *Meas. Sci. Technol.*, vol. 21, no. 4, p. 045101, Apr. 2010.

[23] Y. Chen, X. Zhang, T. Luo, X. Liu, and W. Huang, "Fabrication and characterization of areal roughness specimens for applications in scanning probe microscopy," *Meas. Sci. Technol.*, vol. 24, no. 5, p. 055402, May 2013.

[24] G. M. Sacha, "Influence of the substrate and tip shape on the characterization of thin films by electrostatic force microscopy," *IEEE Trans. Nanotechnol.*, vol. 12, no. 2, pp. 152–156, Mar. 2013.

[25] H. Itoh, T. Fujimoto, and S. Ichimura, "Tip characterizer for atomic force microscopy," *Rev. Sci. Instrum.*, vol. 77, no. 10, p. 103704, Oct. 2006.

[26] T. Inaba, J. Xie, R. Sugiyama, and Y. Homma, "Tip characterizer for atomic force microscopy using singly suspended carbon nanotube," *Surf. Interface Anal.*, vol. 44, no. 6, pp. 690–693, Jun. 2012.

[27] J. S. Villarrubia, "Algorithms for scanned probe microscope image simulation, surface reconstruction and tip estimation," *J. Res. Nat. Inst. Stand. Technol.*, vol. 102, no. 4, pp. 425–454, Jul. 1997.

[28] L. S. Dongmo, J. S. Villarrubia, S. N. Jones, T. B. Renegar, M. T. Postek, and J. F. Song, "Experimental test of blind tip reconstruction for scanning probe microscopy," *Ultramicroscopy*, vol. 85, no. 3, pp. 141–153, Nov. 2000.

[29] D. Necas and P. Klapetek, "Gwyddion: An open-source software for SPM data analysis," *Cent. Eur. J. Phys.*, vol. 10, no. 1, pp. 181–188, Feb. 2012.

[30] J. J. Wu, "Spectral analysis for the effect of stylus tip curvature on measuring rough profiles," *Wear*, vol. 230, no. 2, pp. 194–200, May 1999.

[31] Y. Chen and W. Huang, "Influences of geometrical factors on quantitative surface roughness evaluations by atomic force microscopy," *J. Nanosci. Nanotechnol.*, vol. 9, no. 2, pp. 893–896, Feb. 2009.

[32] K. L. Westra and D. J. Thomson, "Effect of tip shape on surface roughness measurements from atomic force microscopy images of thin films," *J. Vac. Sci. Technol. B*, vol. 13, no. 2, pp. 344–349, Mar. 1995.

Yuhang Chen received the B.S. and Ph.D. degrees in precision instrumentation from the University of Science and Technology of China, Hefei, China.

He is currently an Associate Professor with the Department of Precision Machinery and Precision Instrumentation, University of Science and Technology of China. His current research interests include atomic force microscopy, surface nanometrology, and high-density data storage.

Tingting Luo received the B.S. degree from the Hefei University of Technology, Hefei, China. She is currently working toward the Ph.D. degree in the Department of Precision Machinery and Precision Instrumentation, University of Science and Technology of China, Hefei.

Her current research interests include photoelectric sensing and surface nanometrology.

Wenhao Huang received the B.S. degree in precision instrumentation from Tsinghua University, Beijing, China.

Since 1978, he has been with the Department of Precision Machinery and Precision Instrumentation, University of Science and Technology of China, where he is currently a Professor. His current research interests include femtosecond laser micro/nanofabrication, nanometrology, and standardization.